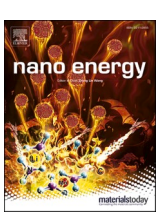
ELSEVIER

Contents lists available at ScienceDirect

Nano Energy

journal homepage: www.elsevier.com/locate/nanoen





Tunning the linkage of structure units to enable stable spinel-based cathode in the wide potential window

Weiyuan Huang ^a, Mingjian Zhang ^{a,*}, Tongchao Liu ^b, Wenguang Zhao ^a, Lunhua He ^{c,d,e}, Liang Yin ^f, Zhijian Tan ^{d,g}, Cong Lin ^a, Jiajie Liu ^a, Qi Zhao ^a, Cong Chen ^a, Rui Qi ^a, Changjian Zuo ^a, Haibiao Chen ^b, Hai Lin ^a, Xinhua Liu ^{i,*}, Khalil Amine ^b, Feng Pan ^{a,*}

- ^a School of Advanced Materials, Peking University, Shenzhen Graduate School, Shenzhen 518055, China
- ^b Chemical Sciences and Engineering Division, Argonne National Laboratory, Lemont, IL 60439, USA
- ^c Beijing National Laboratory for Condensed Matter Physics, Institute of Physics, Chinese Academy of Sciences, Beijing 100190, China
- ^d Spallation Neutron Source Science Center, Dongguan 523803, China
- ^e Songshan Lake Materials Laboratory, Dongguan 523808, China
- f X-ray Science Division, Advanced Photon Source, Argonne National Laboratory, Lemont, IL, 60439, USA
- g Institute of High Energy Physics, Chinese Academy of Sciences, Beijing, China
- ^h Institute of Marine Biomedicine, Shenzhen Polytechnic, Shenzhen 518055, China
- ⁱ School of Transportation Science and Engineering, Beihang University, Beijing 100191, China

ARTICLE INFO

Keywords: Lithium ion batteries Spinel-based cathodes Local structural linkage Restricted Jahn-Teller distortion High energy density

ABSTRACT

The low practical capacity (<140 mA h g $^{-1}$) of spinel phase LiMn $_{2-x}$ Ni $_x$ O $_4$ (0 < x < 1) excludes it from high energy density lithium ion batteries (LIBs) for powering electric vehicles. Extending the operating potential window from 3.0 to 4.8 V to 2.0–4.8 V can double the capacity, but result in fast capacity decay due to the drastic cubic-tetragonal phase transition below 3.0 V, induced by serious Jahn-Teller (J-T) distortion of structure units (Mn $^{3+}$)O $_6$ octahedra. Herein, we propose a novel strategy to suppress J-T distortion by tuning the linkage of structure units MnO $_6$ octahedra. The original full-vertex-sharing LiO $_4$ tetrahedra around MnO $_6$ octahedra in spinel phase are partially replaced by edge-sharing LiO $_6$ octahedra, which relate Mn-O bonds along the d_{xy} plane, thus significantly mitigating J-T distortion and suppressing the phase transition when discharged to 2.0 V. Following this strategy, the prepared spinel-based cathode achieves a high reversible capacity of about 290 mA h g $^{-1}$ and an energy density up to 957 W h kg $^{-1}$ with improved cycling stability. This work finds a new opportunity for the traditional spinel cathode towards applications in high energy density LIBs in a low cost and sustainable manner.

1. Introduction

To cope with the growing demand of lithium ion batteries (LIBs) in electric vehicles (EVs) and power grid energy storage system (PGESS), one of the key challenges is to design cathode materials with low cost and high energy density [1–3]. Compared with the prevailing Co- and Ni-based layered cathode materials, such as LiCoO₂ and LiNi_{1-x-y}Co_xMn_yO₂ (0 \leq x + y \leq 0.5), Mn-based spinel oxide LiMn₂O₄ attracted a wide range of attention due to the low cost and acceptable operation voltage [4–6]. LiMn₂O₄ has been widely used in portable power banks, but absent from EVs and PGESS due to the low energy density (<500 W h kg⁻¹). With partial substitution of Mn by Ni, spinel

LiMn $_{2-x}$ Ni $_x$ O $_4$ (0 < x < 1) (LMNO) exhibits an extra potential plateau close to 4.7 V contributed by the Ni $^{2+}$ /Ni $^{4+}$ redox couple, pushing the energy density up to 580 W h kg $^{-1}$ [7–10]. Nevertheless, the relatively low capacity (<140 mA h g $^{-1}$) can be further improved, since only Li ions at the 8a sites of the spinel framework can be reversibly inserted/extracted. To obtain higher capacity, one approach is to extend the potential window from 3.0 to 4.8 V to 2.0–4.8 V because extra Li ions can be intercalated into the 16c sites below 3.0 V. In this process, Mn $^{4+}$ would be reduced to a lower valence state close to Mn $^{3+}$, which induces serious Jahn-Teller (J-T) distortion and the drastic phase transformation from cubic phase to tetragonal phase (1T) [11,12]. The large lattice volume change as well as the big anisotropic strain due to the decrease of

E-mail addresses: zhangmj@pkusz.edu.cn (M. Zhang), liuxinhua19@buaa.edu.cn (X. Liu), panfeng@pkusz.edu.cn (F. Pan).

^{*} Corresponding authors.

W. Huang et al. Nano Energy 89 (2021) 106457

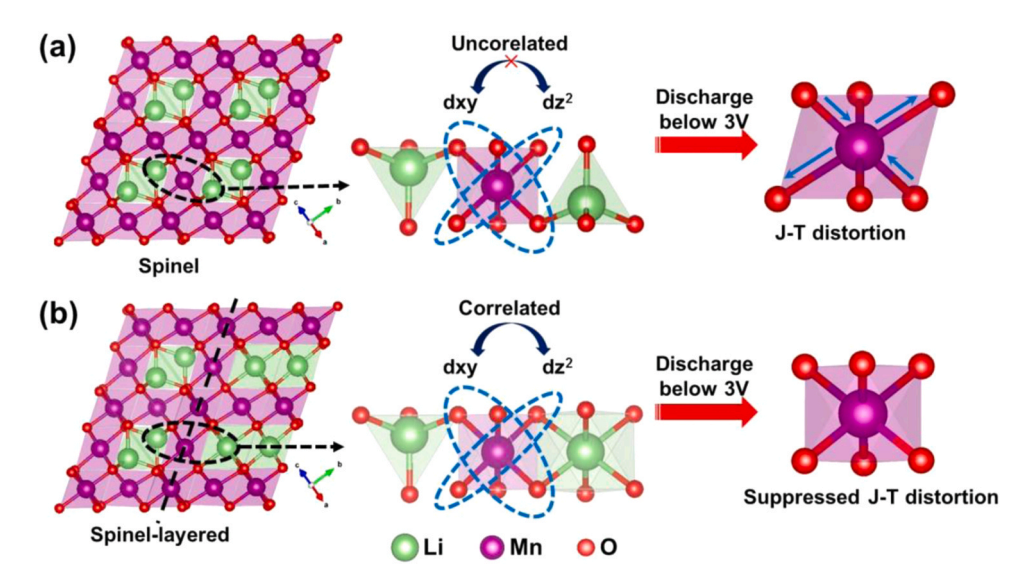
lattice symmetry, would induce cracks in the bulk, then cause loss of electric contact and structural degradation, and eventually the capacity decay. Therefore, inhibiting the cubic-tetragonal phase transformation by suppressing J-T distortion is the key to improve the cycling stability below 3.0 V.

For long, research efforts in spinel cathode are mainly focused on further improving the structural stability, by substitution of Mn or Ni with Li [6,13], Mg [14,15], Al [16], Ti[17,18] or Cr [19], etc., and surface modifications [20-22]. Tarascon and co-workers reported that, considered partially substituted of Mn by lower valent cations could increase the concentration of Mn⁴⁺ in the spinel cathodes, leading to the improved cycling stability [13]. Nevertheless, these strategy just improves the cycling stability above 3.0 V, but still fails below 3.0 V, wherein almost double Li ions insert into the spinel framework with the formation of more Mn³⁺. Actually, few reports are concerned with the improvement of the cycling stability below 3.0 V as we know. Yang's group used Ti to partially replace Ni, and suppressed the J-T effect to some extent utilizing the stronger covalent Ti-O bonds within TiO₆ octahedra, which stabilizes the anion framework and enables the better cycling stability.[17] Another effective approach was reported by our group very recently. Cationic disordering was introduced in LiMn₂O₄ spinel phase to alleviate the cooperative J-T distortion (CJTD), and greatly improved the stability below 3.0 V [23]. Nevertheless, there are still concerns to be resolved. The capacity still suffered a fast decay (only \sim 150 mA h g⁻¹ after 50 cycles) in the Yang's work. In our case, the average voltage decreased markedly with the improved capacity, resulting into a limited improvement in the energy density (~600 W h kg^{-1}). Therefore, extending the available potential range to <3.0 V for spinel cathode is still a critical challenge.

To solve this conundrum, the structural origin for the phase transformation must be carefully figured out. As shown in Scheme 1a, one individual MnO_6 octahedron in spinel $LiMn_2O_4$ was picked out to observe the local environment around it. It is clear that, one MnO_6 octahedron is edge-sharing with six neighboring MnO_6 octahedra, and vertex-sharing with six neighboring LiO_4 tetrahedra. When discharged to below 3 V, the valence of the Mn cations in MnO_6 becomes <+3.5, and all MnO_6 octahedra synergistically stretch along the dz^2 direction due to the J-T effect, dragging the whole anion framework to distort to the tetragonal phase. In this case, the structural changes in the dz^2 direction and dxy plane are uncorrelated in the MnO_6 octahedron because their vertexes are not linked to the same structural unit. If we can correlate the two Mn-O bonds along the dz^2 direction with the four Mn-O bonds in dxy plane by edge-sharing or face-sharing linkage with a

neighboring structural unit, the J-T effect within MnO₆ octahedron is expected to be significantly suppressed, and the unpleasant phase transformation may be alleviated or even inhibited (Scheme 1b). Following this idea, we notice that the TMO₆ octahedra (TM, transition metal) are edge-sharing with neighboring LiO₆ octahedra in layered oxides and they should be able to resist J-T distortion. Furthermore, since the patterns of oxygen cubic close packing are similar in the layered phase and the spinel phase, it is feasible to fuse these two phases together to form a phase complex. Croy and Thackeray et al. introduced spinel phase to Li-rich layered oxides to form a 'layered- layered- spinel' composite to enhance the structure stability [24,25]. Since the main phase is still the layered structure (spinel phase \sim 15%), thus the prepared composite would still suffer from severe average voltage decay upon cycling, similar with the Li-rich layered cathodes [26-28]. Actually, there are a few reports about incorporating Li-rich layered phase into spinel host [29-31]. Manthiram' group comprehensively investigated the electrochemical performance of layered-spinel composite $xLi[Li_{0.2}Mn_{0.6}Ni_{0.17}Co_{0.03}]O_2-(1-x)Li[Mn_{1.5}Ni_{0.425}Co_{0.075}]O_4$ system and found the composite cathodes with x = 0.25 and 0.5 shows improved cycling stability but with limited initial capacity of <200 mA h g^{-1} [30]. Furthermore, the reported spinel-based composites (spinel phase > 50%) still underwent quick structural degradation in the spinel phase. Why did this happen? After careful examination, we found that in these works the two phases are not linked at the atomic level, evidenced by the peak splitting in XRD patterns [29-31]. In this case, the introduced layered phase imposed negligible effect on stabilizing the spinel phase. Therefore, a structurally uniform complex between the layered phase and the spinel phase is critical to implement the effect of stabilization. In an ideal case, the spinel phase and the layered phase form a solid-solution of basic structural units, wherein the spinel domains are surrounded by the layered domains.

Herein, we designed and successfully prepared a spinel-based material Li $_{1.44} \rm Mn_{1.6} \rm Ni_{0.24} \rm O_4$ (SL-LMNO), uniformly compositing with a small amount of the Li-rich layered phase. In SL-LMNO the local structural links by vertex-sharing around the MnO_6 octahedra are partially replaced by edge-sharing. Such a change in the linkage of structure units greatly suppressed the CJTD as expected, leading to a lower degree of phase transformation, thereby delivering a high capacity of $\sim\!290$ mA h g $^{-1}$ with great cycling stability. The energy density of SL-LMNO cathode reached 957 W h kg $^{-1}$, higher than the traditional LiCoO2 and LiNi $_{1-x\cdot y}\rm Co_x Mn_y O_2$ (0 \leq x + y \leq 0.5) and comparable to Lirich layered oxides, enabling the spinel phase as a promising cathode for batteries in EVs.



Scheme 1. Schematic diagrams to show the strategy of tunning the linkage of structure units MnO₆ octahedra to suppress Jahn-Teller distortion in spinel phase.

2. Results and discussion

2.1. Structure of the spinel-layer phase composite

SL-LMNO was prepared by an ion exchange method and a subsequent reannealing process. X-ray photoelectron spectroscopy (XPS) was performed to investigate the valence states of Mn and Ni. In Fig. S1, the molar ratio of Mn³⁺/Mn⁴⁺ and Ni²⁺/Ni³⁺ were determined to be 0.24/ 0.76 and 0.64/0.36, respectively [32]. A pure spinel compound LiMn_{1.76}Ni_{0.24}O₄ (LMNO) was prepared for comparison (Table S1). SEM images (Fig. S2) demonstrate that, both SL-LMNO and LMNO are composed of spherical secondary particles. The difference is that, the particle size of SL-LMNO is smaller and the surface is much smoother and denser compared to LMNO. To precisely determine the phase composition and the lattice structure of SL-LMNO, both synchrotron high-resolution X-ray diffraction (HRXRD) and time of flight neutron powder diffraction (TOF-NPD) patterns were recorded and combined Rietveld refinement was performed (Fig. 1a and b). The results indicate that, SL-LMNO consists of 83.03% of spinel phase (Fd-3m) and 16.97% of layered phase (C2/m) (Table S2 and S3). No peak splitting is visible in the strongest peak as shown in the inset of Fig. 1a, hinting the composite between the two phases is structurally homogenous. Even the weak peaks in the NPD pattern can be fitted almost perfectly (inset of Fig. 1b), further confirming the structural homogeneity of the phase composite. Noticeably, a large amount of Li ions co-occupied the Mn sites in the spinel phase (0.12 Li⁺ at the 16d site), which has been demonstrated effective in suppressing the J-T distortion in spinel phase [23]. The uniform elemental distribution was validated by SEM-EDS mapping as shown in Fig. S3. To further check the compositing uniformity of two phases in local areas, high-resolution transmission electron microscopy (HRTEM) image and the selected-area fast Fourier transform (FFT) maps are shown in Figs. 1c and S4. Layered phase and spinel phase can be identified in two adjacent nano-domains A and B (marked by a red

rectangle and a green rectangle), respectively, showing the nano-level compositing. Moreover, the same interplanar spacing of 4.75 Å between the (111) planes in the spinel region as that between the (001) planes in the layered region exhibits great structural compatibility between the two phases. In comparison, the LMNO is pure spinel phase confirmed by the HRXRD pattern and Rietveld refinement result (Fig. S5). The interplanar spacing of (111) in LMNO was determined to be 4.74 Å from HRTEM (Fig. S6), consistent with the refined result.

To further investigate the local structure at the atomic level, aberration-corrected scanning transmission electron microscopic (STEM) was conducted. Since the atomic contrast in the TEM images is positively related to the atomic number, the transition metal Mn and Ni can be observed while the light elements Li and O are invisible. As shown in Fig. 1d, layered nano-domain and spinel nano-domain are clearly identified at the atomic level. At the domain boundary, MnO₆ octahedra must be edge-sharing with LiO6 octahedra in the layered region since no structural distortion region can be observed between the two regions. In the layered nano-domain (marked by a red rectangle). the slightly brighter contrast in the Li layers demonstrates a certain amount of Li/TM disordering in the Li layers, which is consistent with the refined result (Table S4). The crystal structure is presented on the right panel for a clearer visualization. In the spinel nano-domain (marked by a green rectangle), the spot missing (there supposed to be a third lower peak in the intensity profile) within a slab (marked in the orange box) suggests that, the TM cation at the 16d site of the spinel structure is substituted by Li ion. According to the refinement result, there is 12% of Li/TM mixing at the 16d site in spinel phase (Table S5). Such Li/TM mixing can also create edge-sharing linkage at the neighboring MnO₆ octahedra, thus suppressing the J-T distortion. In one word, atomic-level uniform compositing of layered phase and spinel phase with Li/TM disordering is realized, tuning the linkage of MnO₆ octahedra from full vertex-sharing to partial edge-sharing at the phase boundary.

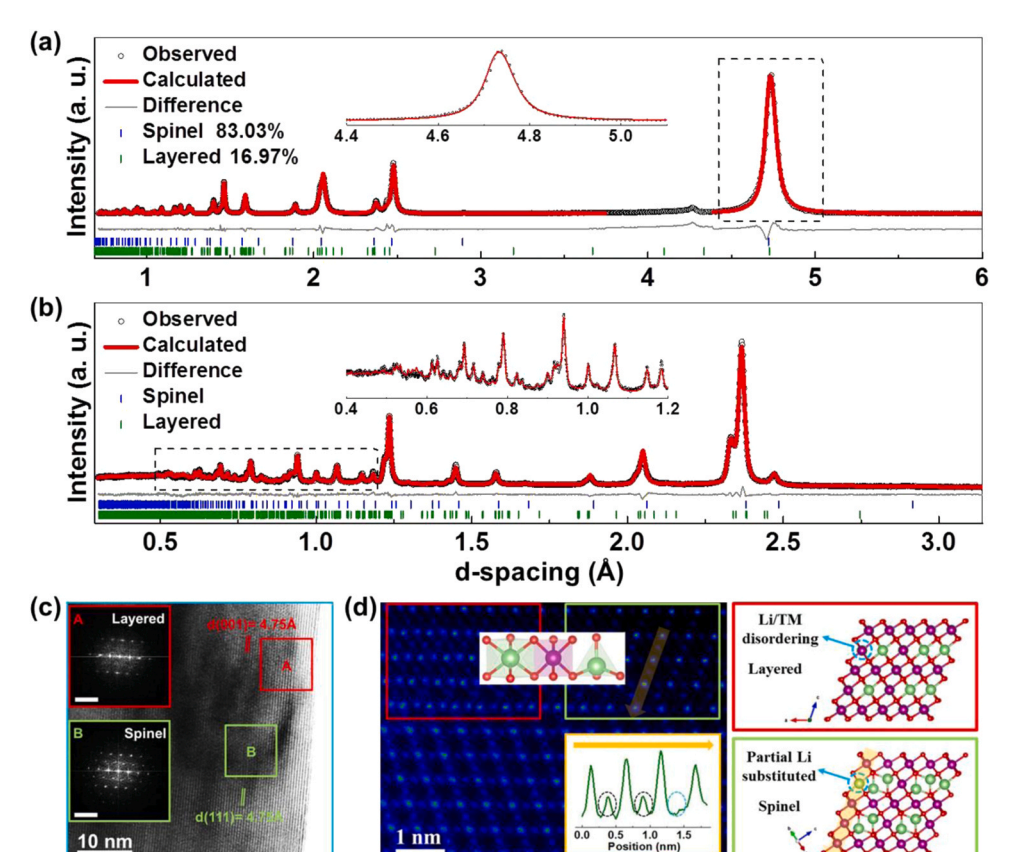


Fig. 1. Structural determination of as-prepared spinel-based cathode SL-LMNO with MnO6 octahedra edge-sharing with LiO6 octahedra. (a) HRXRD and (b) TOF-NPD patterns of SL-LMNO and the combined Rietveld refinement results. The overall R_{wp} is 6.31%. Insets are enlarged from the corresponding regions marked by dashed rectangles. (c) HRTEM image of SL-LMNO. The insets are the corresponding FFT maps of the selected regions. (d) HAADF-STEM image of SL-LMNO. Insets are the linkage mode around MnO6 octahedron and the intensity profile of the selected atomic slab (marked by the yellow arrow). The corresponding atomic structures in the two typical regions are presented on the right panel.

2.2. Enhanced cycling stability

To evaluate the effects of the modified local structural linkage on the electrochemical performance, SL-LMNO as well as the counterpart LMNO were used as cathodes in half-cells and their electrochemical performance was systematically evaluated. (see details in Experimental Section). Fig. 2a displays the charge-discharge curves of SL-LMNO and LMNO cathodes at 0.1 C (1 C = 200 mA h g⁻¹). Typically, there are two potential plateaus at around 4.1 V and 4.7 V for spinel LMNO, which can be associated with Mn³⁺/Mn⁴⁺ and Ni²⁺/Ni⁴⁺ redox couples, respectively. In sharp contrast, two differences from LMNO were observed for SL-LMNO. One is the extended plateau around 4.6 V during the first charge (marked by the green shadow), which should originate from the anionic oxidation in the layered phase [21,33-36]. The oxygen oxidation in the layered phase was confirmed by the O2 release measured using differential electrochemical mass spectrometry (DEMS) test (Fig. S7). The other difference is an extra slope at around 3 V during the discharge process (marked in the blue shade), which can be associated with Li⁺ intercalation into the layered phase [37]. The SL-LMNO cathode delivered a discharge capacity of 290 mA h g⁻¹, about 88% of the theoretical capacity (324 mA h g⁻¹), and slightly higher than MNO (280 mA h g⁻¹) The corresponding dQ/dV profiles were shown in

Fig. 2b-c. Compared with the LMNO, there is an extra oxidation peak at 4.6 V in the 1st cycle for SL-LMNO (marked by the green shadow), which can be assigned to the anionic oxidation process related to layered phase. Furthermore, another pair of redox peaks at 3.2 V (marked in the blue shade) can be related to the Mn³⁺/Mn⁴⁺ redox reaction of the layered phase. These observations were further supported by the cyclic voltammetry (CV) measurements. In Fig. S8a, LMNO exhibits three sharp peaks at around 4.05 V, 4.65 and 4.75 V during the first charge, which can be ascribed to the $Mn^{3+} \rightarrow Mn^{4+}$ and $Ni^{2+} \rightarrow Ni^{3+} \rightarrow Ni^{4+}$ oxidation reactions. During the discharge process, the corresponding reduction peaks can be observed at slightly lower voltages. Until discharged below 3 V, two peaks appear at about 2.70 V and 2.10 V, corresponding to the $Mn^{4+} \rightarrow Mn^{3+}$ reduction process. For SL-LMNO, a new broad reduction peak is observed at 3.2 V (marked by the blue shade), corresponding to the extra plateau in Fig. 2a, and can be ascribed to $Mn^{4+} \rightarrow Mn^{3+}$ reduction process in the layered phase (Fig. S8b). In addition, a pair of much sharper peaks at around 4.7 V is observed (marked by arrows), consistent with the extended plateau above 4.5 V (Fig. 2a). The rate capabilities of the samples were evaluated from 0.1 C to 20 C. As shown in Fig. 2d, SL-LMNO exhibited the similar rate capability as LMNO. Rate test results indicate that, the kinetics of Li⁺ (de)intercalation in the composite was not affected by the introduced

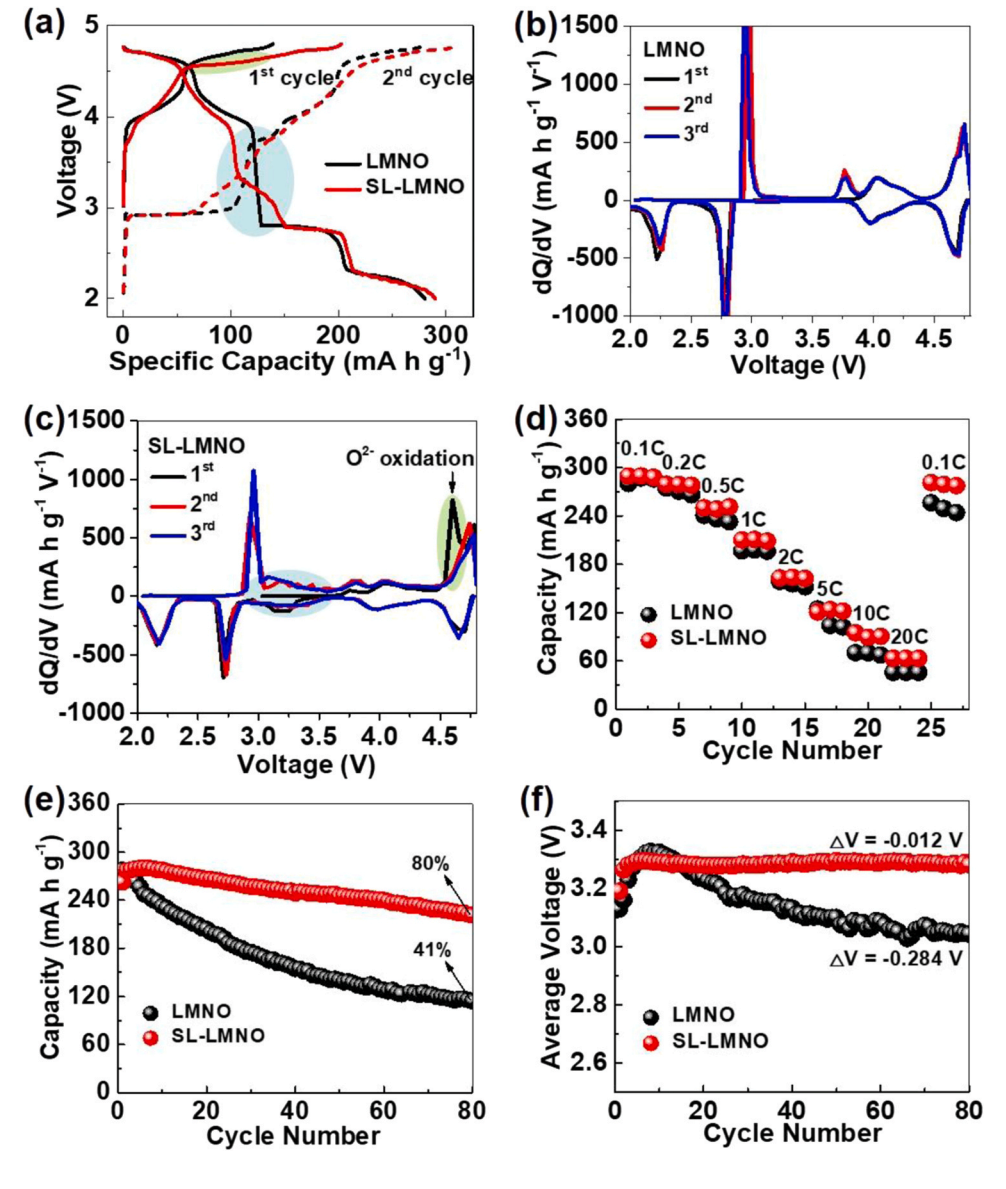


Fig. 2. The comparison of the electrochemical performance for the designed spinel-based composite SL-LMNO and the conventional spinel LMNO. (a) The charge-discharge profiles of LMNO and SL-LMNO in the voltage range of 2.0–4.8 V at 0.1 C (1 C = 200 mA h g⁻¹). The dQ/dV curves of LMNO (b) and SL-LMNO (c) during the initial three cycles. (d) The rate capability of LMNO and SL-LMNO. (e) The plots of discharge capacity as a function of the cycle number for LMNO and SL-LMNO at 0.25 C. (f) the plots of the average voltage as a function of the cycle number for LMNO and SL-LMNO.

layered phase. The slightly higher capacities of SL-LMNO than those of LMNO at higher rates can be ascribed to the better cycling stability. Long-term cycling stability for the two cathodes was also compared. As shown in Fig. 2e, SL-LMNO can retain a discharge capacity of 222 mA h g⁻¹ after 80 cycles at 0.25 C with a capacity retention of 80%, higher than LMNO with a capacity retention of 41%. More interestingly, the decay in the average voltages of SL-LMNO was negligible, about 0.013 V after 80 cycles, much smaller than that of LMNO (0.284 V, Fig. 1f). The observation is different from the severe decay in the average voltage during cycling of typical Li-rich layered oxides [26-28]. The cycling test result hints a stabilization effect of the incorporated layered phase on the spinel phase. This electrochemical performance is better than all reported high capacity spinel-based cathode materials summarized in Table S6. The charge-discharge profiles of LMNO and SL-LMNO cathodes in the 5th, 10th, 20th, 50th and 80th cycles were compared in Fig. S9, and they clearly show the improved capacity and voltage stability in SL-LMNO.

2.3. Suppressed J-T distortion and phase transition

To validate that J-T distortion is suppressed by introducing the edgesharing linkage of structure units, in situ high energy synchrotron XRD (HEXRD) was applied to monitor the real time structural evolutions during the charge/discharge process. As shown in Fig. 3a and b, there was no emergence of new peaks for LNMO and SL-LMNO when discharged from 4.8 V to 3.0 V, hinting no phase transformation. When further discharged to below 3.0 V, both of them experienced transformation from spinel phase to 1T phase, as identified by the representative peaks correlated with 1T phase (marked by dashed ellipses). Nevertheless, an apparent difference is observed: the starting point of phase transformation for SL-LMNO is 2.19 V, 0.54 V lower than that for LMNO (2.73 V), indicating a significant suppression on J-T effect. Furthermore, the strongest peaks of SL-LMNO, consisting of the (111)_S peak of the spinel phase and the (001)_L peak of the layered phase, did not split during the whole charge/discharge process, indicating a high degree of structural compatibility between the layered phase and the

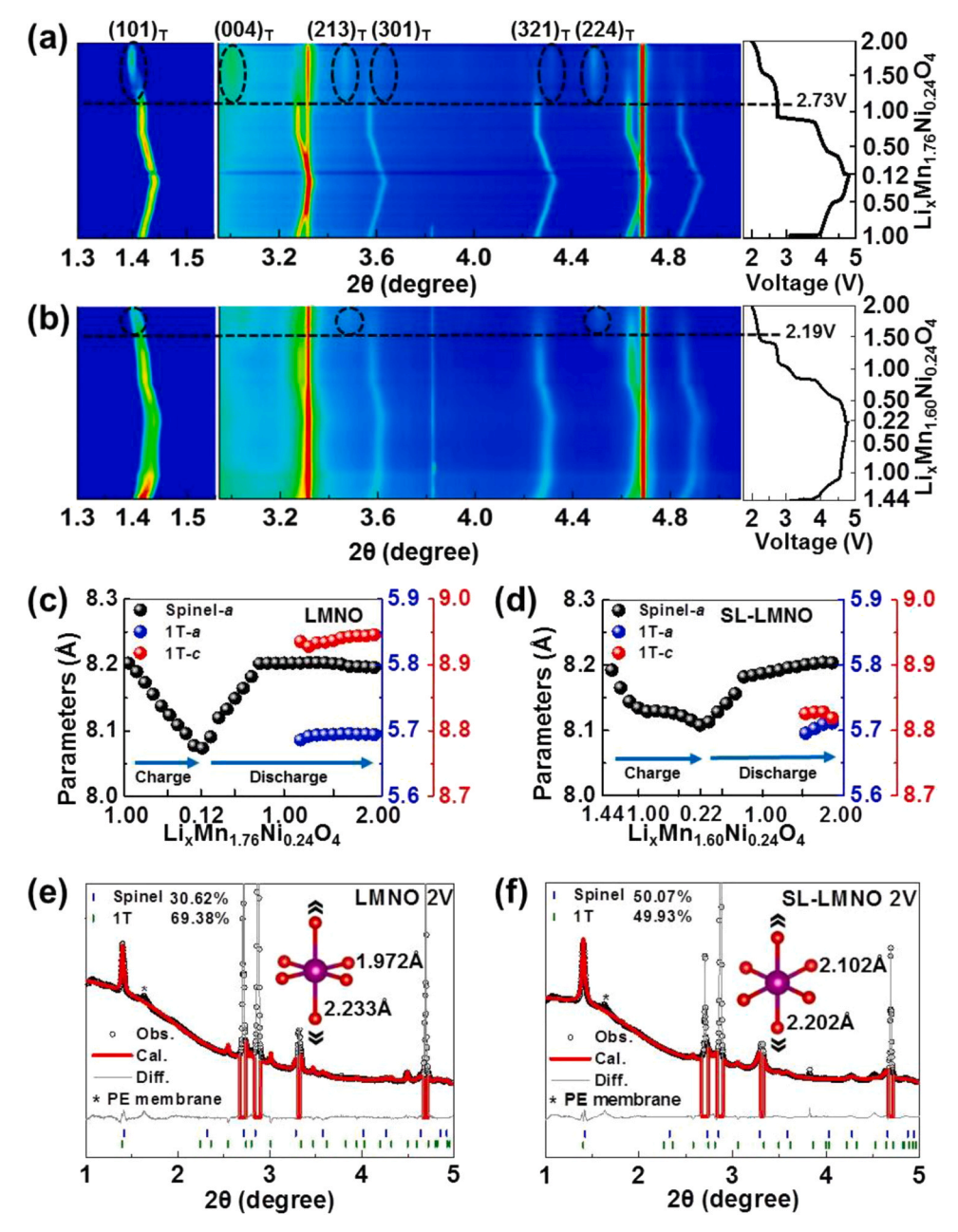


Fig. 3. Suppressed J-T distortion and phase transition in the designed spinel-based composite SL-LMNO. In situ synchrotron HEXRD patterns and the corresponding charge and discharge profiles during the first cycle of (a) LMNO and (b) SL-LMNO. The dashed red lines are used to mark the starting point for the cubic-tetragonal phase transition. The refined lattice parameters, including lattice parameter a of spinel phase (Spinel-a), parameters a and c of the tetragonal phase (marked by 1T-a and 1T-c) during the in situ cycling of (c) LMNO and (d) SL-LMNO. Rietveld-refined XRD patterns of (e) LMNO and (f) SL-LMNO when discharged to 2 V. The insets represent the corresponding MnO₆ octahedra in the formed 1T phase.

spinel phase. Another worth-mentioning point is that strongest peak shifted to the right upon charge and to the left upon discharge, consistent with the behavior of spinel phase [38,39], but opposite to that of layered oxides [40,41]. This result is not only consistent with the majority of the spinel phase, also confirms the high degree of structural homogeneity between the two phases. The similar phenomenon is observed in the *in situ* HEXRD patterns during the 2nd cycle (Fig. S10a-b), confirming the good reversibility of the structural transformation and the suppressed J-T distortion in SL-LMNO. The *ex situ* XRD patterns of SL-LMNO at different charge/discharge states during the 1st cycle can further confirmed the *in situ* observations (Fig. S11).

The lattice parameters were obtained by Rietveld refinements with quantitative analysis. As shown in Fig. 3c and d, parameter a of the spinel phase in LMNO (black dots) underwent a linear decrease with charge, and increased linearly with discharge. After discharged to 3.9 V, a remained nearly constant till the end of the discharge. The maximum variation of a was around 1.7% during charge/discharge process. In contrast, parameter a of the spinel phase in SL-LMNO experienced an overall similar but gentler change with a smaller variation of 1.2%. Another apparent difference is the parameter c of the 1T phase (red dots). The value of c in SL-LMNO was around 8.82 Å, smaller than that in LMNO (8.95 Å). Since the value of c is related to the extent of distortion of the MnO₆ octahedra along the dz^2 direction (Fig. S12), a smaller c value reflects a suppressed J-T effect in SL-LMNO. The similar phenomenon can also be found in the 2nd charge/discharge (Fig. S10c-d).

To better understand the structural evolution, Rietveld refinements were performed on the XRD patterns of LMNO and SL-LMNO when discharged to 2.0 V (Fig. 3e and f, Table S7). LMNO was composed of 30.62% of spinel phase and 69.38% of 1T phase, while SL-LMNO contained less 1T phase (49.93%) at 2.0 V. In order to obtain direct evidence of the J-T distortion in the 1T phase, all Mn-O bond lengths within MnO₆ octahedra were derived from the refinement. In LMNO, the Mn-O bond lengths along the dz^2 direction and the dxy plane are 2.233 and 1.972 Å (difference about 0.261 Å), respectively. In SL-LMNO, the difference of Mn-O bond lengths was much smaller (about 0.100 Å) than those in LMNO with the corresponding bond lengths of 2.202 Å and 2.102 Å, respectively. Therefore, we can conclude that, tunning the linkage of structure units MnO₆ octahedra from vertex-sharing to edgesharing not only decreases the extent of the phase transformation and the content of 1T phase, but also efficiently mitigates the extent of J-T distortion in the newly-formed 1T phase. The electrochemical impedance spectroscopy (EIS) results of LMNO and SL-LMNO before cycling and after 1st, 3rd, 5th cycle were displayed in Fig. S13. The impedance of LMNO exhibits a slight increase after cycles, which may be related to the surface electrolyte decomposition and the irreversible structure transformation. By contrast, the SL-LMNO exhibits a continuously decreased impedance in the initial cycles, which should be due to the improvement of the interfacial structure and bulk structure activation process related with the intergrown layered phase.

2.4. Structural stability after long-term cycling

The dQ/dV profiles at the 10th, 20th, and 50th cycles of LMNO and SL-LMNO cathodes were generated to elucidate the electrochemical degradation process during cycling. As shown in Fig. S14a, all reduction peaks of LMNO at 2.2 V, 2.8 V, 4.0 V and 4.7 V (marked by green arrows) suffer severe decays, suggesting a continuous structure degradation process with the cycle number. In contrast, the corresponding reduction peaks of SL-LMNO in Fig. S14b only show insignificant attenuation except for the peak around 4.7 V. The reduction peak around 4.7 V for SL-LMNO slowly shifts to the lower voltage in contrast to the complete disappearance of the corresponding peaks for LMNO since the 20th cycle, which could be ascribed to the incomplete inhibition of the phase transformation from spinel phase to 1T phase. In addition, the weak and broad peaks at 2.8–3.4 V correlating with the incorporated layered phase, was observed to gradually shift to the lower

voltage during cycling. Such a phenomenon can be assigned to the partial phase transformation from layered phase to spinel phase, which has been widely reported in Li-rich layered oxides [42]. The XRD patterns of LMNO and SL-LMNO after 50 cycles were displayed in Fig. S15. As for LMNO, it shows less T1 phase formation compared with that after the 1st cycle. It indicates that, less Li ions can be inserted into the lattice, which is consistent with the capacity degradation of LMNO after long cycles. In contrast, SL-LMNO after 50 cycles shows negligible Bragg peak change compared with that after the 1st cycle, confirming the great structure stability and the excellent reversibility of phase transformation. The morphology of the LMNO and SL-LMNO electrodes after 50 cycles were studied by SEM. As shown in Fig. S16, the LMNO particle surface is covered with thick decomposition species, and some of secondary particles are broken up into nanoparticles. In comparison, the SL-LMNO particles can still keep original morphology integrity even after long cycles.

In order to better understand the change in the microstructure, HRTEM was used to analyze the local structures of LMNO and SL-LMNO cathodes after 50 cycles. In Figs. 4a and \$18, lots of micro-cracks and lattice distortion can be clearly observed in the cycled LMNO. More details can be examined in the higher magnification HRTEM image (Fig. 4b). A rock-salt like phase showing the (111) planes with the dspacing of 2.40 Å can be identified in region A while in region B the spinel structure persists. While for SL-LMNO, there are no detectable lattice distortions or cracks (Fig. 4c). The HRTEM images and the selected-area FFT maps (Fig. 4d) demonstrate that, SL-LMNO still maintained a complex structure with layered phase and spinel phase after 50 cycles. ICP-OES was conducted to detect the elemental ratio in the cycled LMNO and SL-LMNO samples. As shown in Table S8, the decreased molar ratio between Mn and Ni can be related to the Mn dissolution in the cycled LMNO sample, while SL-LMNO shows an almost negligible change. The Nyquist plots in Fig. S19 compare the electrochemical resistance of LMNO and SL-LMNO samples after 50 cycles. The CEI resistance and charge transfer resistance of SL-LMNO, deduced from the fitting results, are about 6.0 and 32.4 Ω , respectively, much lower than that of LMNO (43.6 and 99.3 Ω , respectively). The lower CEI resistance of SL-LMNO is consistent with the thinner CEI film in the TEM observations (Figs. 4b, d, and S17). The difference in the resistance is consistent with the different extents of structural and electrochemical degradation.

Finally, we propose an explanation based on all above observations in Fig. 4e, to successfully validate our design, *i. e.*, tuning the linkage of structure units to improve structural stability of spinel phase. As shown in the upper panel of Fig. 4e, the spinel phase with vertex-sharing MnO_6 octahedra would undergo severe J-T effect when discharged below 3.0 V, leading to a serious phase transformation to 1T phase. The change in the lattice transforming from spinel phase to 1T phase is significant, and strains accumulate at the phase boundaries, resulting in lots of cracks and rock-salt phase at the particle surface, and finally the poor electrochemical stability. In comparison (the lower panel), as the J-T distortion is greatly suppressed by partially edge-sharing MnO_6 octahedra in the spinel-based material, there is less phase transformation, thereby a smaller extent of lattice mismatch and less strain accumulation, which improves the stability of the spinel phase even after long-term cycling.

3. Conclusions

Based on the in-depth analysis into the linkage of structure units in spinel phase, we successfully designed and fabricated a new spinel-based cathode SL-LMNO, which contains $\rm MnO_6$ octahedra partially edgesharing with $\rm LiO_6$ octahedra, in contrast to the conventional spinel phase LMNO containing $\rm MnO_6$ octahedra fully vertex-sharing with $\rm LiO_4$ tetrahedra. The edge-sharing $\rm LiO_6$ octahedra are able to correlate the Mn-O bonds along the dz^2 direction with those on the dxy plane within the $\rm MnO_6$ octahedra, thereby restricting the Jahn-Teller distortion to a

W. Huang et al. Nano Energy 89 (2021) 106457

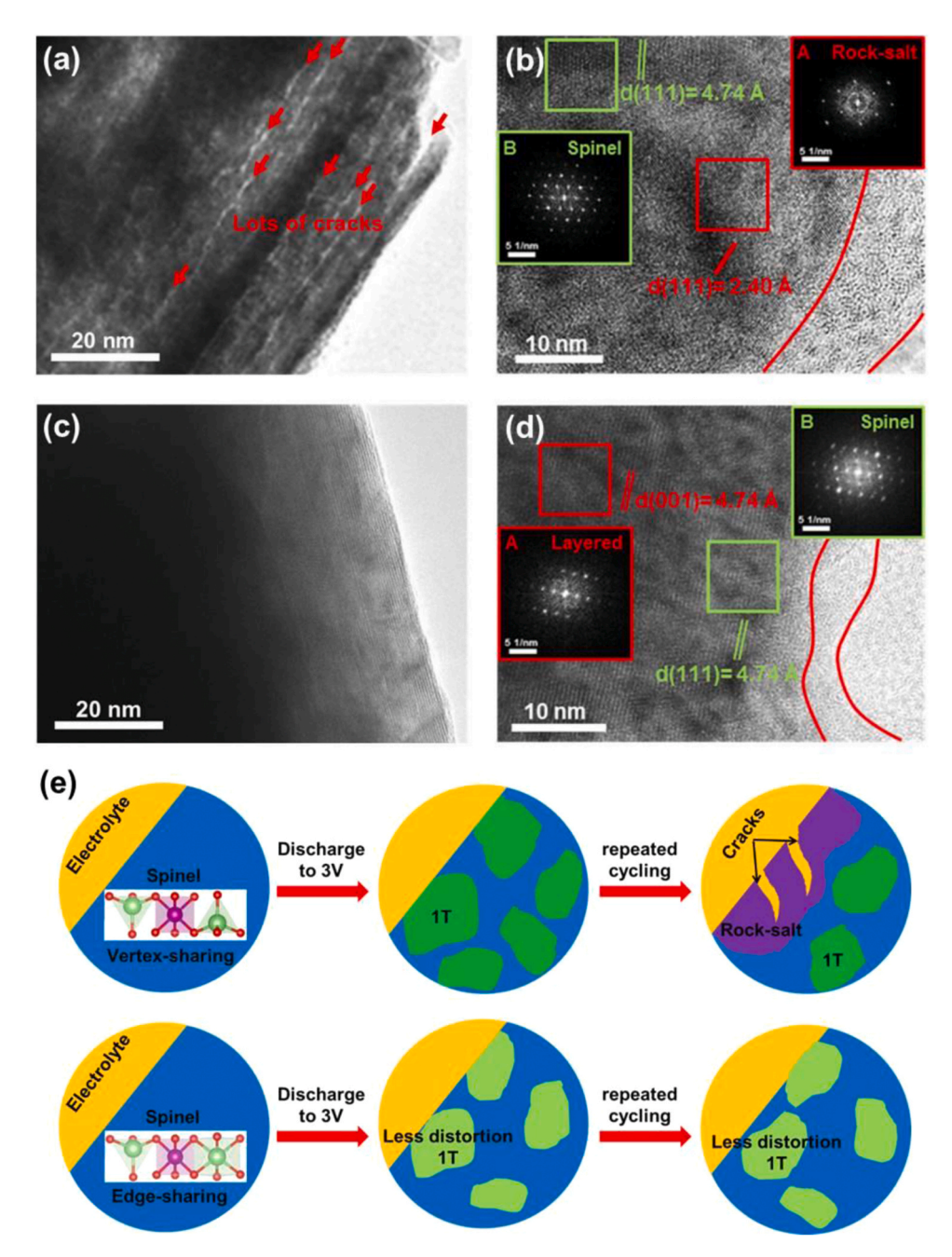


Fig. 4. Long-term structural stability in the designed spinel-based composite SL-LMNO and the conventional spinel LMNO. (a) Low-magnification TEM image and (b) HRTEM images of LMNO after 50 cycles. (c) Low-magnification TEM image and (d) HRTEM images of SL-LMNO after 50 cycles. Insets are the corresponding FFT images of the selected regions. (e) Schematic illustration of the structural stability mechanism by tuning the linkage of structure units MnO₆ octahedra.

great extent. Through the systemic comparison with LMNO, the phase transformation to 1T phase in SL-LMNO was decreased by 20%, and the structural distortion of the $\rm MnO_6$ octahedra in the formed 1T phase was also inhibited. Thus a high reversible capacity of 290 mA h g $^{-1}$ with decent cycling stability was realized for the spinel-based cathode in the wide voltage window of 2.0–4.8 V, increasing the energy density to >900 W h kg $^{-1}$. Our findings not only provide a new strategy to push the traditional spinel cathode to the high-energy-density application, such as batteries for EVs and grid-level energy storage, but more importantly highlight the significant role of structural design in developing next-generation cathodes.

CRediT authorship contribution statement

Weiyuan Huang: Conceptualization, Investigation, Visualization, Methodology, Formal analysis, Writing – original draft. Mingjian Zhang*: Conceptualization, Investigation, Visualization, Formal analysis, Writing – review & editing. Tongchao Liu: Resources. Wenguang Zhao: Resources. Lunhua He: Resources. Liang Yin: Resources. Zhijian Tan: Resources. Cong Lin: Formal analysis. Jiajie Liu: Investigation. Qi Zhao: Investigation. Cong Chen: Investigation. Rui Qi: Investigation. Changjian Zuo: Investigation. Haibiao Chen: Writing – review & editing. Hai Lin: Resources. Xinhua Liu*: Writing – review & editing. Khalil Amine: Resources. Feng Pan: Writing – review & editing, Supervision, Project administration, Funding acquisition.

Declaration of Competing Interest

The authors declare that they have no known competing financial interests or personal relationships that could have appeared to influence the work reported in this paper.

Acknowledgments

This work was financially supported by the National Key R&D Program of China (2016YFB0700600), the Shenzhen Science and Technology Research Grant (No. JCYJ20200109140416788), the Chemistry and Chemical Engineering Guangdong Laboratory (Grant No. 1922018), the National Key R&D Program of China (2020YFB0704500), the National Key Research and Development Program of China (No. 2017YFB0701903) and National Natural Science Foundation of China (No. U1832219). This work was also supported by Clean Vehicles, US-China Clean Energy Research Centre (CERC-CVC2) under the US DOE EERE Vehicle Technologies Office. This research used resources of the Advanced Photon Source (11-IDC), a U.S. Department of Energy (DOE) Office of Science User Facility operated for the DOE Office of Science by Argonne National Laboratory under Contract AC02-06CH11357.

Appendix A. Supporting information

Supplementary data associated with this article can be found in the online version at doi:10.1016/j.nanoen.2021.106457.

References

- B. Dunn, H. Kamath, J.-M. Tarascon, Electrical energy storage for the grid: a battery of choices, Science 334 (2011) 928–935.
- [2] J. Lu, Z. Chen, Z. Ma, F. Pan, L.A. Curtiss, K. Amine, The role of nanotechnology in the development of battery materials for electric vehicles, Nat. Nanotechnol. 11 (2016) 1031–1038.
- [3] J. Deng, C. Bae, A. Denlinger, T. Miller, Electric vehicles batteries: requirements and challenges, Joule 4 (2020) 511–515.
- [4] Y. Huang, Y. Dong, S. Li, J. Lee, C. Wang, Z. Zhu, W. Xue, Y. Li, J. Li, Lithium manganese spinel cathodes for lithium-ion batteries, Adv. Energy Mater. 11 (2) (2021) 2000997, https://doi.org/10.1002/aenm.202000997.
- [5] M. Okubo, Y. Mizuno, H. Yamada, J. Kim, E. Hosono, H.S. Zhou, T. Kudo, I. Honma, Fast Li-ion insertion into nanosized LiMn₂O₄ without domain boundaries, ACS Nano 4 (2010) 741–752.
- [6] T. Liu, A. Dai, J. Lu, Y. Yuan, Y. Xiao, L. Yu, M. Li, J. Gim, L. Ma, J. Liu, C. Zhan, L. Li, J. Zheng, Y. Ren, T. Wu, R. Shahbazian-Yassar, J. Wen, F. Pan, K. Amine, Correlation between manganese dissolution and dynamic phase stability in spinel-based lithium-ion battery, Nat. Commun. 10 (2019) 4721.
- [7] Q. Zhong, A. Bonakdarpour, M. Zhang, Y. Gao, J.R. Dahn, Synthesis and electrochemistry of LiNi_xMn_{2-x}O₄, J. Electrochem. Soc. 144 (2019) 205–213.
- [8] R. Santhanam, B. Rambabu, Research progress in high voltage spinel LiNi_{0.5}Mn_{1.5}O₄ material, J. Power Sources 195 (2010) 5442–5451.
- [9] R. Qiao, Y. Wang, P. Olalde-Velasco, H. Li, Y.-S. Hu, W. Yang, Direct evidence of gradient Mn(II) evolution at charged states in LiNi_{0.5}Mn_{1.5}O₄ electrodes with capacity fading, J. Power Sources 273 (2015) 1120–1126.
- [10] H. Liu, G. Liang, C. Gao, S. Bi, Q. Chen, Y. Xie, S. Fan, L. Cao, W.K. Pang, Z. Guo, Insight into the improved cycling stability of sphere-nanorod-like micronanostructured high voltage spinel cathode for lithium-ion batteries, Nano Energy 66 (2019), 104100.
- [11] M. Wagemaker, F.G.B. Ooms, E.M. Kelder, J. Schoonman, G.J. Kearley, F. M. Mulder, Extensive migration of Ni and Mn by lithiation of ordered LiMg_{0.1}Ni_{0.4}Mn_{1.5}O₄ spinel, J. Am. Chem. Soc. 126 (2004) 13526–13533.
- [12] E.-S. Lee, K.-W. Nam, E. Hu, A. Manthiram, Influence of cation ordering and lattice distortion on the charge–discharge behavior of LiMn_{1.5}Ni_{0.5}O₄ Spinel between 5.0 and 2.0 V, Chem. Mater. 24 (2012) 3610–3620.
- [13] G. Amatucci, J.-M. Tarascon, Optimization of insertion compounds such as LiMn₂O₄ for Li-ion batteries, J. Electrochem. Soc. 149 (2002) K31.
- [14] G. Liang, Z. Wu, C. Didier, W. Zhang, J. Cuan, B. Li, K.Y. Ko, P.Y. Hung, C.Z. Lu, Y. Chen, G. Leniec, S.M. Kaczmarek, B. Johannessen, L. Thomsen, V.K. Peterson, W. K. Pang, Z. Guo, A long cycle-life high-voltage spinel lithium-ion battery electrode achieved by site-selective doping, Angew. Chem. Int. Ed. Engl. 59 (2020) 10594–10602.
- [15] M.-H. Liu, H.-T. Huang, C.-M. Lin, J.-M. Chen, S.-C. Liao, Mg gradient-doped LiNi_{0.5}Mn_{1.5}O₄ as the cathode material for Li-ion batteries, Electrochim. Acta 120 (2014) 133–139.
- [16] J.-Y. Piao, Y.-G. Sun, S.-Y. Duan, A.-M. Cao, X.-L. Wang, R.-J. Xiao, X.-Q. Yu, Y. Gong, L. Gu, Y. Li, Z.-J. Liu, Z.-Q. Peng, R.-M. Qiao, W.-L. Yang, X.-Q. Yang, J.

- B. Goodenough, L.-J. Wan, Stabilizing cathode materials of lithium-ion batteries by controlling interstitial sites on the surface, Chem 4 (2018) 1685–1695.
- [17] M. Lin, S.H. Wang, Z.L. Gong, X.K. Huang, Y. Yang, A strategy to improve cyclic performance of LiNi_{0.5}Mn_{1.5}O₄ in a wide voltage region by Ti-doping, J. Electrochem. Soc. 160 (2013) A3036–A3040.
- [18] J.-M. Lim, R.-G. Oh, W. Cho, K. Cho, M. Cho, M.-S. Park, Power characteristics of spinel cathodes correlated with elastic softness and phase transformation for highpower lithium-ion batteries, J. Mater. Chem. A 5 (2017) 3404–3411.
- [19] J. Wang, P. Nie, G. Xu, J. Jiang, Y. Wu, R. Fu, H. Dou, X. Zhang, High-voltage LiNi_{0.45}Cr_{0.1}Mn_{1.45}O₄ cathode with superlong cycle performance for wide temperature lithium-ion batteries, Adv. Funct. Mater. 28 (2018), 1704808.
- [20] H. Deng, P. Nie, H. Luo, Y. Zhang, J. Wang, X. Zhang, Highly enhanced lithium storage capability of LiNi_{0.5}Mn_{1.5}O₄ by coating with Li₂TiO₃ for Li-ion batteries, J. Mater. Chem. A 2 (2014) 18256–18262.
- [21] B. Xiao, J. Liu, Q. Sun, B. Wang, M.N. Banis, D. Zhao, Z. Wang, R. Li, X. Cui, T. K. Sham, X. Sun, Unravelling the role of electrochemically active FePO₄ coating by atomic layer deposition for increased high-voltage stability of LiNi_{0.5}Mn_{1.5}O₄ cathode material, Adv. Sci. (Weinh.) 2 (2015), 1500022.
- [22] Y. Kwon, Y. Lee, S.O. Kim, H.S. Kim, K.J. Kim, D. Byun, W. Choi, Conducting polymer coating on a high-voltage cathode based on soft chemistry approach toward improving battery performance, ACS Appl. Mater. Interfaces 10 (2018) 29457–29466.
- [23] C. Zuo, Z. Hu, R. Qi, J. Liu, Z. Li, J. Lu, C. Dong, K. Yang, W. Huang, C. Chen, Z. Song, S. Song, Y. Yu, J. Zheng, F. Pan, Double the capacity of manganese spinel for lithium-ion storage by suppression of cooperative Jahn–Teller distortion, Adv. Energy Mater, 10 (2020), 2000363.
- [24] J.R. Croy, J.S. Park, Y. Shin, B.T. Yonemoto, M. Balasubramanian, B.R. Long, Y. Ren, M.M. Thackeray, Prospects for spinel-stabilized, high-capacity lithium-ion battery cathodes, J. Power Sources 334 (2016) 213–220.
- [25] B.R. Long, J.R. Croy, J.S. Park, J. Wen, D.J. Miller, M.M. Thackeray, Advances in stabilizing 'Layered-Layered' xLi₂MnO₃·(1-x)LiMO₂ (M=Mn, Ni, Co) electrodes with a spinel component, J. Electrochem. Soc. 161 (2014) A2160–A2167.
- [26] J. Yang, L. Xiao, W. He, J. Fan, Z. Chen, X. Ai, H. Yang, Y. Cao, Understanding voltage decay in lithium-rich manganese-based layered cathode materials by limiting cutoff voltage, ACS Appl. Mater. Interfaces 8 (2016) 18867–18877.
- [27] E. Hu, X. Yu, R. Lin, X. Bi, J. Lu, S. Bak, K.-W. Nam, H.L. Xin, C. Jaye, D.A. Fischer, K. Amine, X.-Q. Yang, Evolution of redox couples in Li- and Mn-rich cathode materials and mitigation of voltage fade by reducing oxygen release, Nat. Energy 3 (2018) 690–698.
- [28] A. Singer, M. Zhang, S. Hy, D. Cela, C. Fang, T.A. Wynn, B. Qiu, Y. Xia, Z. Liu, A. Ulvestad, N. Hua, J. Wingert, H. Liu, M. Sprung, A.V. Zozulya, E. Maxey, R. Harder, Y.S. Meng, O.G. Shpyrko, Nucleation of dislocations and their dynamics in layered oxide cathode materials during battery charging, Nat. Energy 3 (2018) 641–647.
- [29] A. Bhaskar, S. Krueger, V. Siozios, J. Li, S. Nowak, M. Winter, Synthesis and characterization of high-energy, high-power spinel-layered composite cathode materials for lithium-ion batteries, Adv. Energy Mater. 5 (2015), 1401156.
- [30] E.-S. Lee, A. Huq, H.-Y. Chang, A. Manthiram, High-voltage, high-energy layered-spinel composite cathodes with superior cycle life for lithium-ion batteries, Chem. Mater. 24 (2012) 600–612.
- [31] J. Lee, Q. Zhang, J. Kim, N. Dupre, M. Avdeev, M. Jeong, W.S. Yoon, L. Gu, B. Kang, Controlled atomic solubility in Mn-rich composite material to achieve superior electrochemical performance for Li-ion batteries, Adv. Energy Mater. 10 (2019), 1902231.
- [32] M.X. Lin, L.B. Ben, Y. Sun, H. Wang, Z.Z. Yang, L. Gu, X.Q. Yu, X.Q. Yang, H. F. Zhao, R.C. Yu, M. Armand, X.J. Huang, Insight into the atomic structure of high-voltage spinel LiNi_{0.5}Mn_{1.5}O₄ cathode material in the first cycle, Chem. Mater. 27 (2015) 292–303.
- [33] R.A. House, G.J. Rees, M.A. Pérez-Osorio, J.-J. Marie, E. Boivin, A.W. Robertson, A. Nag, M. Garcia-Fernandez, K.-J. Zhou, P.G. Bruce, First-cycle voltage hysteresis in Li-rich 3d cathodes associated with molecular O₂ trapped in the bulk, Nat. Energy 5 (2020) 777–785.
- [34] G. Assat, D. Foix, C. Delacourt, A. Iadecola, R. Dedryvere, J.M. Tarascon, Fundamental interplay between anionic/cationic redox governing the kinetics and thermodynamics of lithium-rich cathodes, Nat. Commun. 8 (2017) 2219.
- [35] S. Zhao, K. Yan, J. Zhang, B. Sun, G. Wang, Reaction mechanisms of layered lithium-rich cathode materials for high-energy lithium-ion batteries, Angew. Chem. Int. Ed. Engl. 60 (2021) 2208–2220.
- [36] K.E. Madsen, K.A. Wade, R.T. Haasch, D.B. Buchholz, K.L. Bassett, B.G. Nicolau, A. A. Gewirth, Origin of enhanced cyclability in covalently modified LiMn_{1.5}Ni_{0.5}O₄ cathodes, ACS Appl. Mater. Interfaces 11 (2019) 39890–39901.
- [37] J.X. Liu, J.Q. Wang, Y.X. Ni, Y.D. Zhang, J. Luo, F.Y. Cheng, J. Chen, Spinel/lithium-rich manganese oxide hybrid nanofibers as cathode materials for rechargeable lithium-ion batteries, Small Methods 3 (2019), 1900350.
- [38] L. Kondracki, A. Kulka, A. Milewska, J. Molenda, In-situ structural studies of manganese spinel-based cathode materials, Electrochim. Acta 227 (2017) 294–302
- [39] H.M. Wu, J.P. Tu, Y.F. Yuan, Y. Li, X.B. Zhao, G.S. Cao, Electrochemical and ex situ XRD studies of a LiMn_{1.5}Ni_{0.5}O₄ high-voltage cathode material, Electrochim. Acta 50 (2005) 4104–4108.

[40] R.-Z. Yin, Y.-S. Kim, S.-J. Shin, I. Jung, J.-S. Kim, S.-K. Jeong, In situ XRD investigation and thermal properties of Mg doped LiCoO₂ for lithium ion batteries, J. Electrochem. Soc. 159 (2012) A253–A258.

- [41] J.U. Choi, N. Voronina, Y.K. Sun, S.T. Myung, Recent progress and perspective of advanced high-energy Co-less Ni-rich cathodes for Li-ion batteries: Yesterday, today, and tomorrow, Adv. Energy Mater 10 (2020) 2002027, https://doi.org/ 10.1002/aenm.202002027.
- [42] M.J. Zhang, Z.B. Li, L. Yu, D.F. Kong, Y.W. Li, B. Cao, W.G. Zhao, J.G. Wen, F. Pan, Enhanced long-term cyclability in Li-Rich layered oxides by electrochemically constructing a Li_xTM_{3-x}O₄-type spinel shell, Nano Energy 77 (2020), 105188.



Weiyuan Hang received his B.S. degree from South China Normal University in 2017. He is pursuing his Ph.D. degree in the School of Advanced Materials, Peking University, China. His research interests mainly focus on cathode materials for lithium ion batteries and sodium ion batteries, especially on layered oxide materials including Mn-rich layered oxides and high voltage LiCoO₂ layered oxides.



Dr. Mingjian Zhang got his Ph.D. degree from Fujian Institute of Research on the Structure of Matter, Chinese Academy of Sciences in 2013, then worked there as an assistant research fellow for one year. From 2014–2018, he was a postdoc in School of Advanced Materials, Peking University, and became an assistant research professor in 2018–2020, and promoted to an associate research professor since 2021. Meanwhile, he was a research scholar in Brookhaven National Lab from 2016 to 2019, then in the University of Chicago in 2019. He has been engaged in the fields of high-performance cathode materials for Li-ion batteries, especially the structural evolution and structure-property research of the cathodes.



Dr. Tongchao Liu currently works as a Postdoctoral Appointee at Argonne National Laboratory. He obtains his Ph.D. degree from Peking University in 2019. His research interests are focused on the interface of electrochemistry, cathode materials and materials characterization, in particular, concentration gradient cathode design and fundamental understanding of failure chemistries through in-situ synchrotron-based X-ray techniques.



Wenguang Zhao is an engineer in the School of Advanced Materials, Peking University Shenzhen Graduate School, China. He has over 10 years' experience in material characterization using wide range of analytical tools including XRD, XPS, SEM and TEM. His research interests mainly focus on the Ex/in-situ TEM and Ex/in-situ XRD characterization of battery materials.



Dr Lunhua He is team leader of General Purpose Powder Diffractometer (GPPD) at CSNS. She received her Ph.D. degree in 2002 in condensed Matter Physics from State Key Laboratory for Magnetism, Institute of Physics, Chinese Academy of Sciences, Beijing, P.R. China. She was responsible for the design and construction of GPPD. The scientific goal of GPPD is to provide a flexible and versatile powder diffractometer for a wide range of novel materials development and discovery. Her current research interests focused on the studies of neutron diffraction and scattering of magnetic materials and battery materials.



Dr. Liang Yin is a Postdoctoral Researcher at the X-ray Science Division of Argonne National Laboratory. He obtained his Ph. D. degree from Stony Brook University in 2019. He has rich experience in the structural analysis at multi length scales using both X-ray and neutron scattering. His research mainly focuses on the identification of structural defects and the Ex/insitu structural evolutions in battery materials during thermal treatments or electrochemical tests.



Dr. Zhijian Tan is an assistant researcher at CSNS. He received his B.S. degree and M.Sc degree from Sun Yat-Sen University. Then he received his Ph.D. degree from The Graduate University for Advanced Studies in Japan and worked as a post-doctoral fellow at High Energy Accelerator Research Organization (KEK), Japan. His research interests focus on anomalous thermal expansion materials.



Cong Lin received his B.S. and Ph.D. degree in chemistry from Chongqing University and Peking University in 2013 and 2018, respectively. From 2018 to early 2021, he worked as a post-doctor in Prof. Feng Pan's group in Peking University Shenzhen Graduate School, and is currently a postdoctoral fellow in The Hong Kong Polytechnic University. His research interest mainly focuses on the structures of novel functional materials and their relationship with properties and performances.



Jiajie Liu is currently a Ph.D. candidate in Prof. Feng Pan's group at Peking University Shenzhen Graduate School, China. He received his B.S. degree in Chemistry from Peking University in 2016. Currently his research interests focus on high energy density cathode materials for Li-/Na-ion batteries, especially on layered oxide materials including Li- and Mn-rich layered oxides and Ni-rich layered oxides.

W. Huang et al. Nano Energy 89 (2021) 106457



Qi Zhao is currently pursuing his M. Sc. degree under the supervision of Prof. Feng Pan at Peking University Shenzhen Graduate School, China. He received B. Sc. from Nankai University in 2019. His research interests mainly focus on investigating the relation between the structure of cathode materials for Li-ion batteries and their electrochemical behavior.



Hai Lin is vice dean of School of Advanced Materials, Peking University Shenzhen Graduate School. He is responsible for the testing and characterization platform of new materials, and focusing on the evaluation and industrial application development of clean energy materials and devices.



Cong Chen is currently pursuing his M.Sc degree under the supervision of Prof. Feng Pan at Peking University Shenzhen Graduate School, China. He received his B.Eng. from South China University of China in 2018. His research interests mainly concentrate on study the relationship between structure and property, and modifying strategies of Na iron anode material.



Dr. Xinhua Liu is lecture of School of Transportation Science & Engineering at Beihang University, Visiting Lecture of Dyson School of Design Engineering at Imperial College London (UK), lab manager of Beihang University (Zhejiang) New Energy Vehicle Institute. Her research interests mainly lie in the interface between electrochemical science and engineering applying a digital process, including designing energy materials for various energy storages; model-driven microstructure optimization for high performance batteries; cloud control based battery degradation mechanism, diagnose and battery management system design.



Rui Qi is currently pursuing his M.Sc. degree under the supervision of Prof. Feng Pan at Peking University Shenzhen Graduate School, China. He received his B.Eng. from Central South University in 2018. His research interests mainly focus on investigating the relation between the structure of cathode materials for Li- and Na-ion batteries and their electrochemical behavior.



Dr. Khalil Amine is an Argonne Distinguished Fellow and the leader of the Advanced Battery Technology team at Argonne National Laboratory, where he is responsible for directing the research and development of advanced materials and battery systems for HEV, PHEV, EV, and satellite applications. He is an adjunct professor at Stanford University. Among his many awards, Dr. Amine is the 2019 reception of the prestigious Global Energy Prize. He is a six-time recipient of the R&D 100 Award, which is considered as the Oscar of technology and innovation. He is an ECS fellow, and associate editor of the journal of Nano-Energy.



Changjian Zuo is currently pursuing his M. Sc. degree under the supervision of Prof. Feng Pan at Peking University Shenzhen Graduate School, China. He graduated from Soochow university and received his B. S. degree from the School of Shangang Iron and Steel in 2018. His research interests focus on the cathode materials of lithium ion batteries.



Dr. Feng Pan, founding Dean of School of Advanced Materials, Peking University Shenzhen Graduate School, got B.S. from Dept. Chemistry, Peking University in 1985 and Ph.D. from Dept. of P&A Chemistry, University of Strathclyde, Glasgow, UK, with "Patrick D. Ritchie Prize" for the best Ph.D. in 1994. With more than a decade experience in large international incorporations, Prof. Pan has been engaged in fundamental research and product development of novel optoelectronic and energy storage materials and devices. As Chief Scientist, Prof. Pan led eight entities in Shenzhen to win 150 million RMB grant for the national new energy vehicles (power battery) innovation project since 2013.



Haibiao Chen is currently a senior researcher at School of Advanced Materials, Peking University Shenzhen Graduate School. He received his Bachelor's degree from Tsinghua University in 2000 and PhD from Stevens Institute of Technology in 2006. He worked at Velocys during 2006–2011 and UES during 2011–2014.